

Research Paper

Electronic Conductance Modulation of Armchair Graphyne Nanoribbon by Twisting Deformation

Somayeh Fotoohi^{*1}, Mansoureh Pashangpour², Saeed Haji-Nasiri³

¹ Department of Electrical Engineering, Islamshahr Branch, Islamic Azad University, Islamshahr, Iran

² Department of Physics, Islamshahr Branch, Islamic Azad University, Islamshahr, Iran

³ Faculty of Electrical, Biomedical and Mechatronics Engineering, Qazvin Branch, Islamic Azad University, Qazvin, Iran

Received: 10 Apr. 2023

Revised: 02 Jun. 2023

Accepted: 05 Jun. 2023

Published: 10 Jun. 2023

Use your device to scan and
read the article online



Keywords:

**α -Graphyne Nanoribbon,
Twisting Deformation,
Transmission; Molecular
Energy Spectrum,
Transmission Pathways**

Abstract

The electronic and transport properties of armchair α -graphyne nanoribbons (α -AGyNRs) are studied using density functional theory with non-equilibrium Green function formalism. The α -AGyNRs are considered with widths $N = 6, 7$ and 8 to represent three distinct families behavior in presence of twisting. The band structure, current-voltage characteristic, transmission spectra, molecular energy spectrum, molecular projected self-consistent Hamiltonian (MPSH), and transmission pathways are studied for α -AGyNRs with $\theta = 0^\circ, 30^\circ, 60^\circ$ and 90° . The results indicate that 6 and 7 α -AGyNRs devices are semiconductor, while 8 α -AGyNR device has metallic character. Moreover, these behaviors are preserved by applying the twist. Our theoretical study shows that the electronic conduction of α -AGyNRs can be tuned by twisted deformation. The maximum modulation of conductance at 1.2 V is obtained 69.94% for 7 α -AGyNR device from $\theta = 0^\circ$ to $\theta = 90^\circ$. The investigation of MPSH demonstrates that distribution of charge density get localized on twisting sites which impact on the electron tunneling across the scattering region.

Citation: Somayeh Fotoohi, Mansoureh Pashangpour, Saeed Haji-Nasiri
Electronic Conductance Modulation of Armchair Graphyne Nanoribbon by Twisting
Deformation. **Journal of Optoelectrical Nanostructures. 2023; 8 (2): 15-31**

DOI: [10.30495/JOPN.2023.31553.1281](https://doi.org/10.30495/JOPN.2023.31553.1281)

***Corresponding author:** Somayeh Fotoohi

Address: Department of Electrical Engineering, Islamshahr Branch, Islamic Azad University, Islamshahr, Iran. **Email:** s.fotoohi@iaau.ac.ir

1. INTRODUCTION

In recent decades, carbon-based nanomaterials (CBNs) have attracted most attention as a candidate for future electronic applications [1-2]. Various allotropes of carbon have been discovered including graphite [3], fullerenes [4], carbon nanotubes [5-6], and graphene [7-8]. Among of CBNs, graphene has attracted tremendous attention among the scientific community since mechanical exfoliation of graphite using scotch tape in 2004 by Novoselov et al. [8].

Graphene consists of sp^2 hybridized carbon atoms which arrange in two-dimensional (2D) planar honeycomb lattice. Graphene has extraordinary mechanical behaviors and unique electronic properties such as high mechanical flexibility, high specific surface area, outstanding electrical conductivity, excellent carrier mobility which make it valuable for applications in future nanodevices [9-15]. By changing the sp^2 carbon bonds proportion in graphene to the acetylenic linkages (C–C≡C–C), another novel 2D carbon allotrope can be designed that is known as graphyne (Gy). With different percentages of the C–C≡C–C such as 100%, 66.67%, 33.33% and 41.67%, four typical structures can form namely α -, β -, γ - and 6,6,12-graphynes, respectively [16-21]. After the prediction of the graphyne family by Baughman et al. [16], extensive experimental [20] and theoretical studies [18] have been devoted to explore graphyne's properties and development of its industrial applications [17-25].

Graphyne sheet is patterned via the lithographic technique into nanoribbons (NRs) along two different orientations, which are called armchair (A) and zigzag (Z) graphyne nanoribbons (GyNRs). Their strongly anisotropic electronic properties depend on the width and edge morphology of NR [17, 21]. Furthermore, geometrical formations such as ripple [26-27], wrap [28], fold [29] and twist [30-35] occur inevitably in the production of low-dimensional carbon nanostructures which influences widely on the electronic transport properties. Recently, the twist has been experimentally formed in graphene and graphyne which modifies their physical properties [33-34]. G. P. Tang et al. investigated the twisted deformation on the electronic conduction of armchair and zigzag GNRs. The results indicate that semiconductor GNRs are strictly sensitive to twist while the metallic GNRs have insignificant altering by twisting [32]. However, the effect of twist in GyNRs has not been considered as extensively.

Herein, we have theoretically investigated the influence of twisted deformation on transport properties of α -AGyNRs using the non-equilibrium Green's function (NEGF) method [36] combined with the density functional

theory (DFT) [37-38]. The α -AGyNRs can be divided into three categories with $N = 3p, 3p + 1, 3p + 2$, where p is an integer number. In present work, we choose three α -AGyNRs with various widths ($N = 6, 7, 8$) as examples to cover distinct features of three different groups [17].

The paper is organized as follows: the models and computational methods are given in Section 2. The results of the twisting deformation on the electronic transport properties of 6, 7 and 8 α -AGyNRs are obtained and analyzed in Section 3. Finally, summarizes findings are presented in Section 4.

2. MODELS AND COMPUTATIONAL METHODS

Figure 1 shows planar and twisted α -AGyNRs devices with width of $N=6$ (as an example for representation) which N denotes to the dimmer lines number across the width of ribbon. Each device is partitioned into three sections: left electrode (LE), right electrode (RE) and the central scattering region (SR). Each electrode includes one unit cell along the transport direction and the central scattering region is composed by a super cell with 5 unit cells along the ribbon. The dimensions of 6 α -AGyNR supercell in the X, Y and Z directions are 33.38Å, 15 Å and 60.33 Å, respectively.

The region of central scattering is considered large enough to vanish interaction between the wave functions of electrodes. All carbon of edge atoms are attached to hydrogen atoms. In twisted α -AGyNR device, the electrodes and scattering region are rotated around the center axis (θ).

The electronic and transport properties of structures are performed using the DFT with NEGF method. Norm-conserved Troullier-Martins pseudopotentials are employed to describe interaction between valance and core electrons [39]. The generalized gradient approximation (GGA) of the Perdew-Burke-Ernzerhof (PBE) is used to calculate exchange and correlation energy [40]. The calculations of self-consistent are carried out with a mixing rate of 0.01 and the convergence criterion for the density matrix is considered to be 10^{-4} . The kinetic energy cutoff is chosen to be 150 Ry and a Monkhorst–Pack k-mesh of $1 \times 1 \times 50$ are set in order to obtain good balance between accuracy and calculation efficiency. Optimized geometries of systems are performed until the force on each atom is smaller than $0.02 \text{ eV}/\text{Å}$. We apply periodic boundary conditions along the Z direction and a vacuum of 15 Å imposes to avoid spurious interaction between nanoribbons images in non-periodic directions (i.e. X and Y directions here).

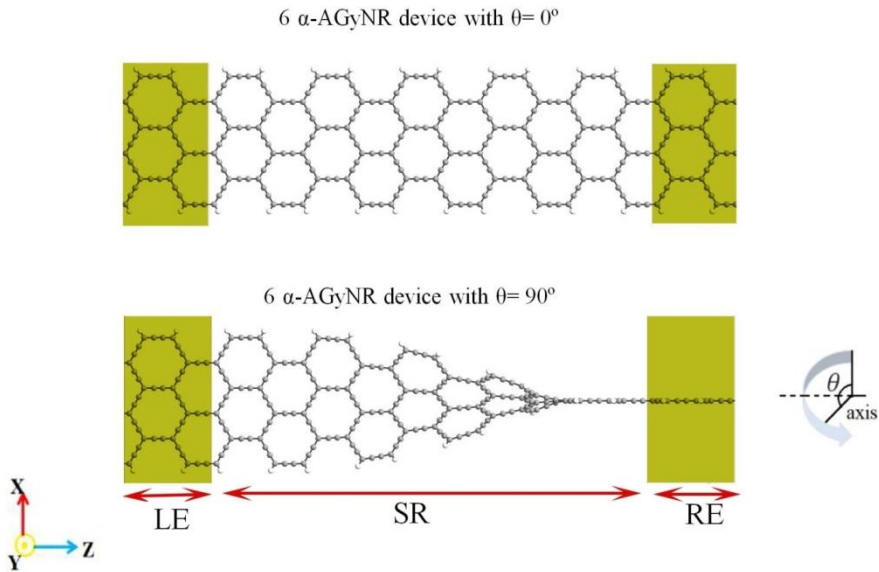


Fig. 1. Schematic models of planar and twisted 6 α -AGyNR devices, respectively. The left electrode (LE), the right electrode (RE) and the scattering region (SR) are represented in this figure. All edge carbon atoms are attached to hydrogen atoms. The θ is the twisted angle around the center axis of α -AGyNRs.

In the two-probe system, the Green function of the complete system with open boundary conditions is calculated from Eq. (1):

$$G(E) = \left[(E + i\eta)I - H - \sum_L(E) - \sum_R(E) \right]^{-1} \quad (1)$$

Here, η is an infinitesimal positive number, and I denotes the identity matrix.

$\sum_{L(R)}$ represents left (right) electrode self-energies using the following equation [36]:

Here, η is an infinitesimal positive number, and I denotes the identity matrix. $\sum_{L(R)}$ represents left (right) electrode self-energies using the following equation [36]:

$$\sum_L(E) = \tau_L^\dagger g_L(E) \tau_L, \sum_R(E) = \tau_R^\dagger g_R(E) \tau_R \quad (2)$$

g_L and g_R are the surface green function of left and right electrode, respectively. τ_L and τ_R represent information about the coupling quality between the central scattering and the electrodes. $\Gamma_{L,R}(E)$ is broadening function of the left (right) electrode based on the following equation:

$$\Gamma_{L,R}(E) = i \left[\sum_{L,R}(E) - \sum_{L,R}^\dagger(E) \right] = -2 \text{Im} \sum_{L,R}(E) \quad (4)$$

The total transmission probability is given by

$$T(E, V_b) = \text{Trace} \left[\Gamma_R(E) G(E) \Gamma_L(E) G^\dagger(E) \right] \quad (5)$$

$G(E)$ and $G^\dagger(E)$ present the retarded and advanced Green's functions, respectively. Current is obtained from the transmission probability using Landauer– Büttiker relation,

$$I(V_b) = \frac{2e}{h} \int_{\mu_L}^{\mu_R} T(E, V_b) [f_L(E) - f_R(E)] dE \quad (6)$$

Where e refers the electron charge, h presents the Planck's constant.

$f_{L,R}(E) = \frac{1}{1 + e^{(E - \mu_{L,R})/KT}}$ is left (right) Fermi function. $\mu_{L,R} = E_f \pm \frac{eV_b}{2}$ is left (right) electrochemical potentials.

3. RESULT AND DISCUSSION

The electronic and transport properties of 6, 7 and 8 α -AGyNRs devices are investigated with twist angles between $\theta = 0^\circ$ and 90° (in steps of 30°) based on the Landauer formula. The current–voltage characteristics of 6, 7 and 8 α -AGyNRs devices in presence of twisted angles of $\theta = 0^\circ, 30^\circ, 60^\circ$ and 90° are presented in Figs. 2(a)-(c). Furthermore, electrodes band structures are presented in the insets of Figs. 2(a)-(c).

Calculated band structures of 6 and 7 α -AGyNRs show that these structures are semiconductor with direct band gap of 0.392 eV and 0.431 eV at Γ point, respectively. It is note that the gap of energy for 7 α -AGyNR is a slightly wider (39 meV) than 6- α -AGyNR. However, 8 α -AGyNR band structure is very distinct from those of the 6 and 7 α -AGyNRs. Valence and conduction bands of 8 α -AGyNR touch the Fermi level at the Γ point and exhibits metallic behavior. These findings are consistent with previously reported results [17].

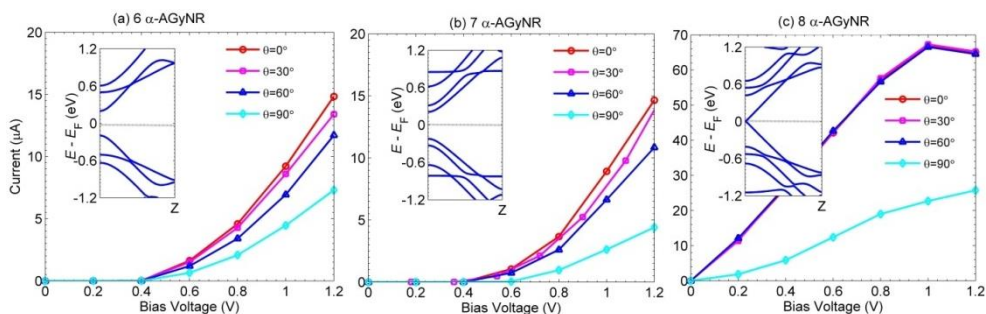


Fig. 2. Plots of current versus bias voltage for (a) 6 α -AGyNR (b) 7 α -AGyNR (c) 8 α -AGyNR devices with $\theta=0^\circ, 30^\circ, 60^\circ$ and 90° . The band structures of planar 6, 7 and 8 α -AGyNRs unit cells are presented in the insets of Figs. 2(a)-(c).

Currents of 6 and 7 α -AGyNR devices with $\theta=0^\circ, 30^\circ, 60^\circ$ and 90° are zero until the bias of ~ 0.4 V, after that the currents increase. This behavior indicates that these systems are semiconductor (Fig. 2(a)-(b)).

On the other hand, the current–voltage characteristics of 8 α -AGyNR devices with $\theta=0^\circ, 30^\circ, 60^\circ$ and 90° display metallic behavior. This is attributed to the number of available conduction channels around the Fermi energy (inset of Fig. 1 (c)) and hence these devices can carry larger currents comparing of 6 and 7 α -AGyNRs devices. Furthermore, the electrical conductivity of 8 α -AGyNR is more than those of the 6, 7 α -AGyNRs under the similar condition.

It can be seen that in Figs. 2(a)-(c), the currents of 6 and 7 α -AGyNR systems decrease by the increasing of twisting angles. In contrast, the current of 8 α -AGyNR has no changes with the increase of twisting angles between 0° to 60° and it decreases at the twisting angle of 90° . One can see that a negative differential resistance (NDR) behavior is discovered in the current-voltage

characteristic of 8 α -AGyNR with twisting angles of 0° , 30° and 60° in [1 V, 1.2 V] bias.

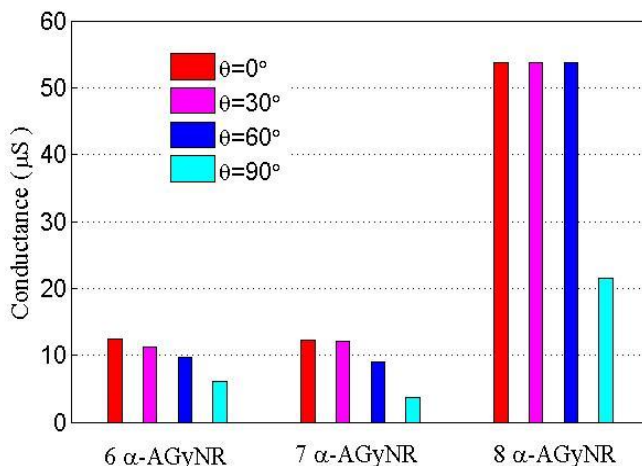


Fig. 3. The conductance of the considered structures at 1.2 V for 6, 7 and 8 α -AGyNR devices with $\theta=0^\circ$, 30° , 60° and 90° .

Conductance of the considered structures at 1.2 V is given for different angles in Fig. 3. As a result, the maximum modulations of conductance at 1.2 V are obtained 50.87%, 69.94% and 60.10% for 6, 7 and 8 α -AGyNRs devices from $\theta=0^\circ$ to $\theta=90^\circ$, respectively.

To gain more insight into the effects of twisting on the transport properties, the transmission spectrum for 6, 7 and 8 α -AGyNR devices are presented with twist angles ($\theta=0^\circ$, 30° , 60° and 90°) in 0 and 1.2 V in Fig. 4.

Transmission spectra for 6 α -AGyNR with $\theta=0^\circ$, 30° , 60° and 90° under $V_b=0$ V have transmission gap about 0.4 eV. Therefore, the transmission probability vanishes for voltages in [0 V, 0.4 V] that results an off-state current.

For 7 α -AGyNR with $\theta=0^\circ$, 30° and 60° , a transmission gap are observed around 0.4 eV. Moreover, gap of transport for 7 α -AGyNR with $\theta=90^\circ$ enhances to 0.6 eV. Thus, there is no current for $\theta=90^\circ$ in [0 V, 0.6 V]

In the case of 8 α -AGyNR with $\theta=0^\circ$, 30° , 60° and 90° , there is no transmission gap under $V_b=0$ V. Furthermore, the coefficients of transmission at 1.2 V have high values around the Fermi level which means better conductive capability than 6 and 7 α -AGyNR devices in the same of twist angles.

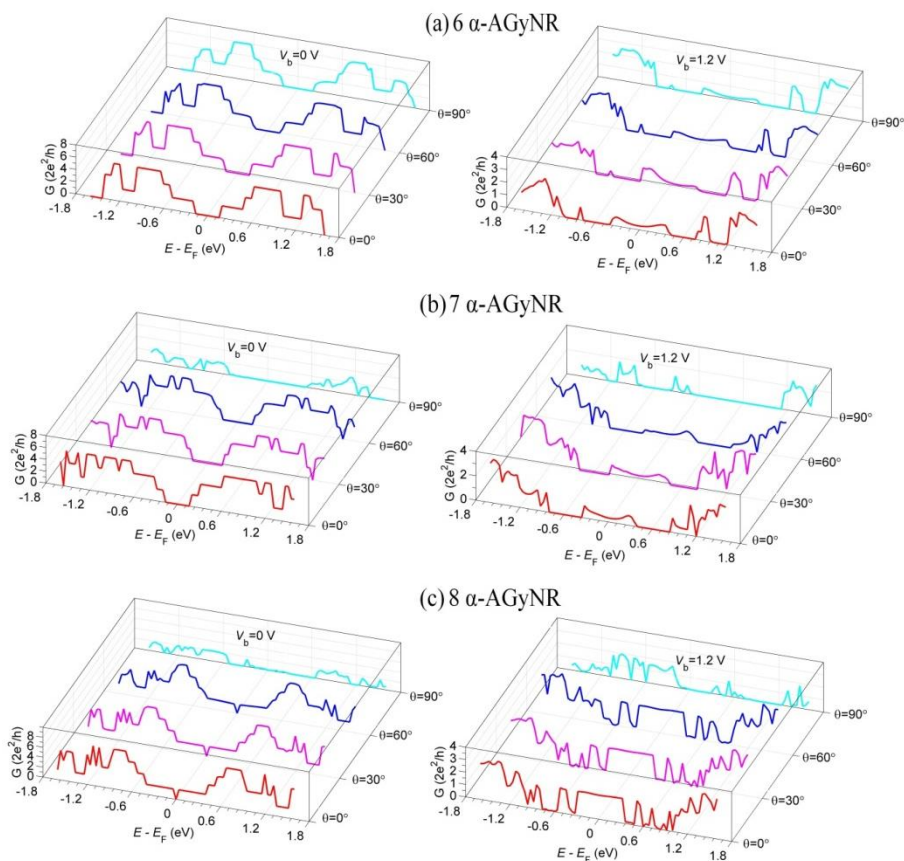


Fig. 4. Transmission spectrum for (a) 6 α -AGyNR (b) 7 α -AGyNR (c) 8 α -AGyNR devices with $\theta=0^\circ, 30^\circ, 60^\circ$ and 90° in the biases of 0 and 1.2 V. The Fermi level is set to zero.

To further understand the twisting influence on transport behavior of α -AGyNRs with different widths, the left and right electrodes band structures for 6, 7 and 8 α -AGyNR devices are illustrated at 1.2 V (Fig. 5). The window of bias is presented by black solid lines and the region of energy band matching has been highlighted in green. In the presence of the external bias across the junction, the left (right) electrodes energy bands move upward (downward) 0.6 eV from the Fermi level. When left and right electrodes bands have an overlap within the window of bias, the transmission of electron occurs from left electrode to right electrode. It is worthy to be pointed out that in the case of 8 α -

AGyNR device, more resonance states appear into the bias window for two electrodes. Whereas, the energy bands of 6 and 7 α -AGyNRs are matched partially in the bias window. This phenomenon has an important impact on quantum transport behavior and the current of device.

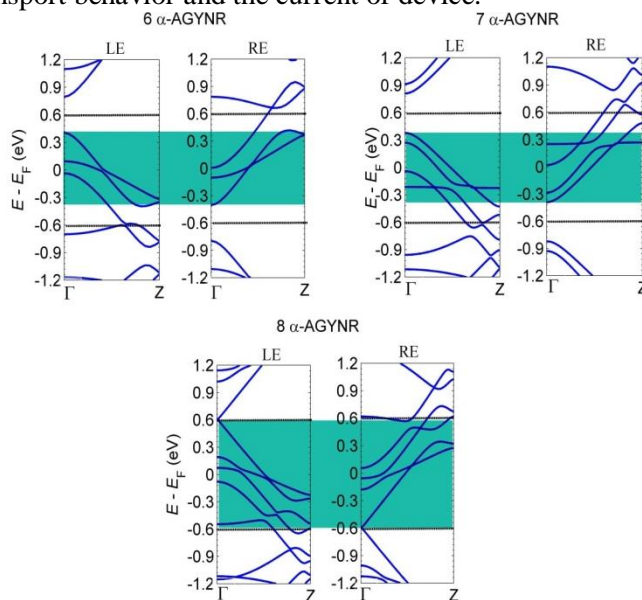
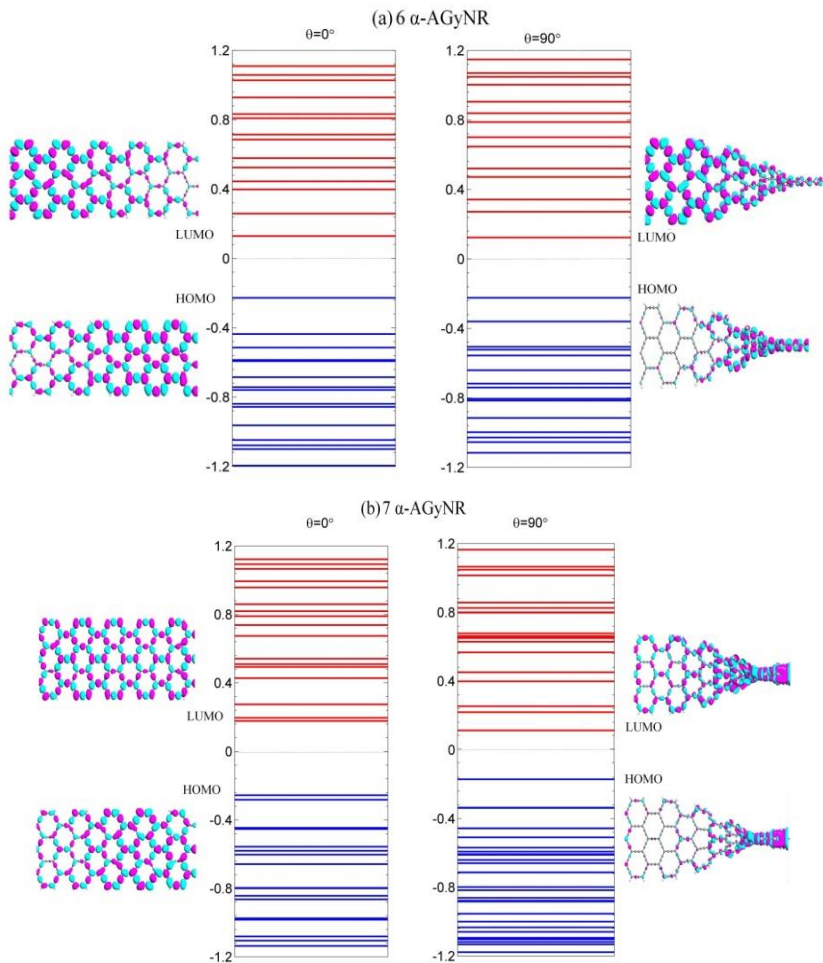


Fig. 5. The LE and RE band structures for 6, 7 and 8 α -AGyNR devices under 1.2 V. The energy band matching region within the bias window has been highlighted in green.

Another important condition for electronic transmission comes from intensity of coupling between scattering region molecular orbitals and the electrodes. The molecular orbitals which have main contribution to the total current are HOMO and LUMO.

The molecular energy spectrum of scattering regions and the MPSH of the HOMO and LUMO for 6, 7 and 8 α -AGyNR devices at 1.2 V are plotted in Fig. 6. One can see that the HOMO and LUMO densities present a notable symmetric distribution in the whole junction for considered devices with $\theta=0^\circ$. In contrast, only the spatial distribution of LUMO is delocalized over the central scattering region in 6, 7 and 8 α -AGyNRs with $\theta=90^\circ$. More importantly, when an electron with the energy of this orbital is entered into the central region, it has a high probability to pass via the central scattering region. Furthermore, spatial distributions of HOMO are entirely localized on twisting sites, hence the

conductance channels are localized close to the right electrode and the current are suppressed.



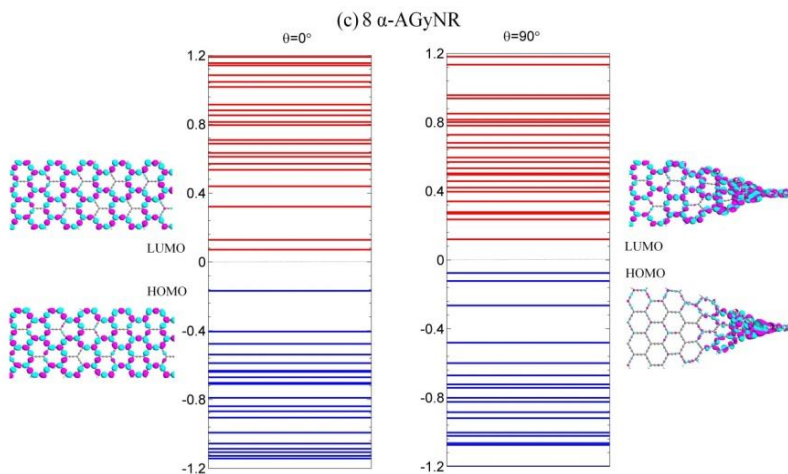


Fig. 6. Molecular energy spectrum of scattering regions for (a) 6 α -AGyNR (b) 7 α -AGyNR (c) 8 α -AGyNR devices at $\theta=0^\circ$ and $\theta=90^\circ$ under 1.2 V. The MPSH of HOMO (lower) and LUMO (upper) for each device are presented. The isovalues are fixed 0.02 for all eigenvalues.

The pathway of transmission is a main tool which disintegrates the coefficient of transmission into local bond contributions (T_{ij}). This can be expressed as follows [41-42]:

$$T(E) = \sum_{i \in A, j \in B} T_{ij}(E) \quad (7)$$

Where T_{ij} describe how the current propagates through the atomic bonds.

The transmission pathways of 6, 7 and 8 α -AGyNRs with $\theta=0^\circ$ and 90° at the Fermi level under 1.2 V bias are illustrated in Fig. 7. In this figure, the thickness of each arrow exhibit the local transmission magnitude between chemical bonds and the direction of arrows show the electron flow. In addition, the density of pathways is illustrated by the volume of the arrows. We can clearly observe that the pathways of transmission for α -AGyNRs devices are specifically dependent on ribbons width. Furthermore, the transport channel number for electrons in planar devices is more than those in the twisting α -AGyNRs. Thus, this result confirms that twisting can reduce the electronic conduction ability of the α -AGyNRs.

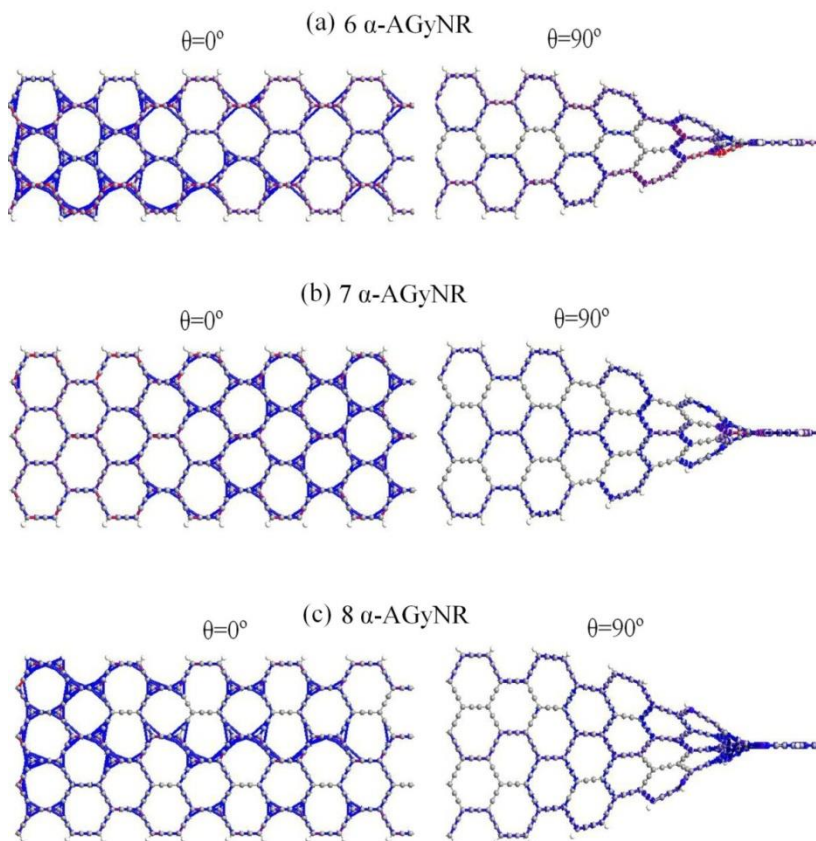


Fig. 7. The transmission pathways of (a) 6 α -AGyNR (b) 7 α -AGyNR (c) 8 α -AGyNR devices with $\theta=0^\circ$ and 90° at the Fermi level under 1.2 V bias.

3. CONCLUSION

We have carried out the calculations to explore the electronic and transport properties of 6, 7 and 8 α -AGyNRs with the planar and twisted geometries. The current-voltage characteristic for semiconductor 6 and 7 α -AGyNRs devices are sensitive to twisting deformations with $\theta=0^\circ$, 30° , 60° and 90° . In addition, threshold voltage of 6 and 7 α -AGyNR devices with $\theta=0^\circ$, 30° and 60° is about 0.4 V. In the case of $\theta=90^\circ$, threshold voltage remains unchanged at 0.4V for 6 α -AGyNR device and it increase to 0.6V for 7 α -AGyNR.

The results show that the current-voltage characteristic of 8 α -AGyNR is almost insensitive by twisting angle of 0° , 30° and 60° , while current significant reduction occurs for $\theta=90^\circ$. The NDR behavior is observed for 8 α -AGyNR with $\theta=0^\circ$, 30° and 60° in the range of [1 V, 1.2 V] bias. Moreover, the current-voltage characteristic for 8 α -AGyNR with $\theta=90^\circ$ exhibits Ohm's law. It is found that the transmission of 8 α -AGyNR with $\theta=0^\circ$, 30° and 60° is around $2G_0$ at Fermi energy, but it is negligible with $\theta=90^\circ$.

The MPSH of LUMO and HOMO for considered devices with $\theta=0^\circ$ exhibit a remarkable symmetric distribution in the scattering region at 1.2 V. However, the distribution of HOMO gets localized on the twisting site with $\theta=90^\circ$. The transmission pathways illustrate that the number of transport channels in 8 α -AGyNR is more than those in 6 and 7 α -AGyNRs with $\theta=90^\circ$.

The maximum modulations of conductance at 1.2 V are calculated 50.87%, 69.94% and 60.11% for 6, 7 and 8 α -AGyNRs devices from $\theta=0^\circ$ to $\theta=90^\circ$, respectively. Our results suggest that the electronic and transport properties of nanodevices can be tuned by applying twisted deformation.

REFERENCES

- [1] S. Yu, T. Teng, C. Huang, H. Hsieh and Y. Wei, *Performance Evaluation of Carbon-Based Nanofluids for Direct Absorption Solar Collector*, *Energies*, 16 (2023, Jan.) 1-17.
Available: <https://doi.org/10.3390/en16031157>
- [2] X. Shi, H. Liu, Z. Hu, J. Zhao, J. Gao, *Porous carbon-based metal-free monolayers towards to high stable and flexible wearable thermoelectric and microelectronics*, *Nanoscale*, 15 (2023, Dec.) 1522-1528. Available: <https://doi.org/10.1039/D2NR05443D>
- [3] L. Yi, K. Noguchi, L. Liu, A. Otsu, T. Onda, Z. Chen, *Deformation behavior of graphite and its effect on microstructure and thermal properties of aluminum/graphite composites*, *Journal of Alloys and Compounds*, 933 (2023, Feb.) 167752.
Available: <https://www.sciencedirect.com/science/article/abs/pii/S0925838822041433>
- [4] S. Zhao, X. Zhang, Y. Ni, Q. Peng, Y. Wei, *Anisotropic mechanical response of a 2D covalently bound fullerene lattice*, *Carbon*, 202 (2023, Jan.) 118-124.

Available: <https://doi.org/10.1016/j.carbon.2022.11.005>

- [5] S. N. Jafari, A. Ghadimi, S. Rouhi, *Strained Carbon Nanotube (SCNT) Thin Layer Effect on GaAs Solar Cells Efficiency*, Journal of Optoelectrical Nanostructures, 4 (2020, Autumn) 87-110.
Available: https://jopn.marvdasht.iau.ir/article_4505.html
- [6] H. H. Madani, M. R. Shayesteh, M. R. Moslemi, *A Carbon Nanotube (CNT)-based SiGe Thin Film Solar Cell Structure*, Journal of Optoelectrical Nanostructures, 6 (2021, Winter) 71-86.
Available: https://jopn.marvdasht.iau.ir/article_4541.html
- [7] A. K. Geim, K. S. Novoselov, *The rise of graphene*, Nature Materials, 6 (March 2007) 183–191.
Available: <https://www.nature.com/articles/nmat1849>
- [8] K.S. Novoselov, A.K. Geim, S.V. Morozov, D. Jiang, Y. Zhang, S.V. Dubonos, I.V. Grigorieva, A.A. Firsov, *Electric Field Effect in Atomically Thin Carbon Films*, science, 306 (2004, Oct.) 666-669.
Available: <https://www.science.org/doi/abs/10.1126/science.1102896>
- [9] M.F. Craciun, S. Russo, M. Yamamoto, S. Taruchac, *Tuneable electronic properties in graphene*, Nanotoday, 6 (2011, Feb.) 42-60.
Available: <https://doi.org/10.1016/j.nantod.2010.12.001>
- [10] J. Wang, F. Ma, W. Liang, M. Sun, *Electrical properties and applications of graphene, hexagonal boron nitride (h-BN), and graphene/h-BN heterostructures*, Materials Today Physics, 2 (2017, Sep.) 6-34.
Available: <https://doi.org/10.1016/j.mtphys.2017.07.001>
- [11] M Pashangpour, V Ghaffari, *Investigation of structural and electronic transport properties of graphene and graphane using maximally localized Wannier functions*, Journal of Theoretical and Applied Physics, 7 (2013, Dec.), 1-8.
Available: https://jtap.srbiau.ac.ir/article_18825.html
- [12] Somayeh Fotoohi, Mohammad Kazem Moravvej-Farshi, Rahim Faez, *Electronic and transport properties of monolayer graphene defected by one and two carbon ad-dimers*, Appl. Phys. A, 116 (2014, Apr.) 2057–2063.
Available: <https://link.springer.com/article/10.1007/s00339-014-8400-9>

- [13] F.V. Alamdarlo, G. Solookinejad, F. Zahakifar, M. R. Jalal, M. Jabbari, *Synthesis of Graphene Oxide Functionalized with Amio Methyl Phosphonic Acid (AMPA) and its Structural Characterization*, Journal of Optoelectrical Nanostructures, 6 (2021, Spring) 91-106.
Available: https://jopn.marvdasht.iau.ir/article_4770.html
- [14] M. Jabbari, M. Dehghan, M. k. moravvej farshi, G. Darvish, M. Ghaffari-miab, *Ultra-Compact Bidirectional Terahertz Switch Based on Resonance in Graphene Ring and Plate*, Journal of Optoelectrical Nanostructures, 4 (Autumn, 2019) 99-112.
Available: https://jopn.marvdasht.iau.ir/article_3761.html
- [15] h. Rahimi, *Absorption Spectra of a Graphene Embedded One Dimensional Fibonacci Aperiodic Structure*, Journal of Optoelectrical Nanostructures, 3 (Autumn, 2018) 45-58.
Available: https://jopn.marvdasht.iau.ir/article_3259.html
- [16] R. H. Baughman, H. Eckhardt, and M. Kertesz, *Structure property predictions for new planar forms of carbon: Layered phases containing sp^2 and sp atoms*, J. Chem. Phys., 87 (Dec. 1987) 6687-6699.
Available: <https://aip.scitation.org/doi/10.1063/1.453405>
- [17] W. Wu, W. Guo and , X. C. Zeng, *Intrinsic electronic and transport properties of graphyne sheets and nanoribbons*, Nanoscale, 5 (2013, Jul.) 9264-9276.
Available: <https://doi.org/10.1039/C3NR03167E>
- [18] S. Lakshmy, A. Kundu, N. Kalarikkal, B. Chakraborty, *Pristine and Transition Metal Decorated Holey Graphyne Monolayer as an Ammonia sensor: Insights from DFT Simulations*, J. Phys. D: Appl. Phys., 56 (2023, Jan.) 055402.
Available: <https://iopscience.iop.org/article/10.1088/1361-6463/aca2e>
- [19] K. Srinivasu and Swapan K. Ghosh, *Graphyne and Graphdiyne: Promising Materials for Nanoelectronics and Energy Storage Applications*, J. Phys. Chem. C, 116 (2012, Jan.), 5951–5956.
Available: <https://doi.org/10.1021/jp212181h>

- [20] X. Liu, S. M. Cho, S. Lin, Z. Chen, W. Choi, Y. Kim, E. Yun, E. H. Baek, D. H. Ryu, H. Lee, *Constructing two-dimensional holey graphyne with unusual annulative π -extension*, *Matter*, 5 (2022, Jul.), 2306-2318.
Available: <https://doi.org/10.1016/j.matt.2022.04.033>
- [21] M Golzani, M Poliki, S Haji-Nasiri, *γ -Graphyne rectifier and NDR tunable by doping, line edge roughness and twist*, *Computational Materials Science*, 190 (2021, Apr.)110303.
Available:<https://www.sciencedirect.com/science/article/abs/pii/S0927025621000288>
- [22] J. Ren, N. Zhang, P. Liu, *Li adsorption on nitrogen-substituted graphyne for hydrogen storage*, *Fullerenes, Nanotubes and Carbon Nanostructures*, 29 (2021, Oct.) 212-217.
Available: <https://doi.org/10.1080/1536383X.2020.1830066>
- [23] D. C. M. Rodrigues, L. L. Lage, P. Venezuela, A. Latge, *Exploring the enhancement of the thermoelectric properties of bilayer graphyne nanoribbons*, *Phys. Chem. Chem. Phys.*, 24 (2022, Apr.), 9324–9332.
Available:<https://pubs.rsc.org/en/content/articlelanding/2022/cp/d1cp05491k>
- [24] Y. Ni, X. Wang, W. Tao, S. Zhu, K. Yao, *The spin-dependent transport properties of zigzag α -graphyne nanoribbons and new device design*, *Scientific Reports*, 6, (2016, May.) 25914.
Available: <https://www.nature.com/articles/srep25914>
- [25] P. Nayebi, M. Shamshirsaz, *Effect of vacancy defects on transport properties of α -armchair graphyne nanoribbons*, *The European Physical Journal B*, 93 (2020, Sep.) 170.
Available:<https://link.springer.com/article/10.1140/epjb/e2020-10183-5>
- [26] J. A. Tallaa, E. A. Almahmoudb, K. Al-Khaza'leha, and H. Abu-Farsakhc, *Structural and Electronic Properties of Rippled Graphene with Different Orientations of Stone-Wales Defects: First-Principles Study*, *Semiconductors*, 55 (2022, Feb.) 643–653.
Available: <https://link.springer.com/article/10.1134/S1063782621070198>
- [27] A. Fasolino, J. H. Los, M. I. Katsnelson, *Intrinsic ripples in graphene*, *Nature Materials*, 6 (2007, Sep.) 858–861.
Available: <https://www.nature.com/articles/nmat2011>

- [28] Y. Huang, L. Zhang, H. Lu, F. Lai, Y. Miao and T. Liu, *A highly flexible and conductive graphene-wrapped carbon nanofiber membrane for high-performance electrocatalytic applications*, *Inorg. Chem. Front.*, 3 (2016, May.) 969-976. Available: <https://pubs.rsc.org/en/content/articlelanding/2016/qi/c6qi00101g>
- [29] C. Lencar, M. Becton, X. Wang, *Computational analysis of hydrogenated graphyne folding*, *Chemical Physics Letters*, 646 (2016, Feb.) 110-118. Available: <https://www.sciencedirect.com/science/article/abs/pii/S0009261416000385>
- [30] M. Saiz-Bretín, F. Domínguez-Adame, A. V. Malyshev, *Twisted graphene nanoribbons as nonlinear nanoelectronic devices*, *Carbon*, 149 (2019, Aug.) 587-593. Available: <https://www.sciencedirect.com/science/article/abs/pii/S0008622319304038>
- [31] S. Yue, Q. Yan, Z. Zhu, H. Cui, Q. Zheng, G. Su, *First-principles study on electronic and magnetic properties of twisted graphene nanoribbon and Möbius strips*, *Carbon*, 71 (2014, May.) 150-158. Available: <https://doi.org/10.1016/j.carbon.2014.01.023>
- [32] G. P. Tang, J. C. Zhou, Z. H. Zhang, X. Q. Deng, and Z. Q. Fan, *Altering regularities of electronic transport properties in twisted graphene Nanoribbons*, *Appl. Phys. Lett.*, 101, (2012, Jul.) 023104. <https://aip.scitation.org/doi/10.1063/1.4733618>
- [33] Y. Saito, J. Ge, K. Watanabe, T. Taniguchi, and A. F. Young, *Decoupling superconductivity and correlated insulators in twisted bilayer graphene*, *Nature Physics*, 16 (2020) 926-930. Available: <https://doi.org/10.48550/arXiv.1911.13302>
- [34] A. Nimbalkar, H. Kim, *Opportunities and Challenges in Twisted Bilayer Graphene: A Review*, *Nano-Micro Letters*, 12 (2020, Jun.) 126. Available: <https://link.springer.com/article/10.1007/s40820-020-00464-8>
- [35] X. Wei, G. Guo, T. Ouyang, and H. Xiao, *Tuning thermal conductance in the twisted graphene and gamma graphyne nanoribbons*, *Journal of Applied Physics* 115, (2014, Apr.) 154313.

Available: <https://aip.scitation.org/doi/10.1063/1.4872136>

- [36] V. Do, *Non-equilibrium Green function method: theory and application in simulation of nanometer electronic devices*, Adv. Nat. Sci: Nanosci. Nanotechnol., 5 (2014, Jun.) 033001.

Available: <https://iopscience.iop.org/article/10.1088/2043-6262/5/3/033001>

- [37] R. M. Dreizler and E. K. U. Gross. *Density Functional Theory* (1990, Springer,).

Available: <https://link.springer.com/book/10.1007/978-3-642-86105-5>

- [38] R. G. Parr, Y. Weitao. *Density-functional Theory of Atoms and Molecules* Oxford University Press, (1994, Jan.).

Available: <https://academic.oup.com/book/41995>

- [39] M. Fuchs, M. Scheffler, *Ab initio pseudopotentials for electronic structure calculations of poly-atomic systems using density-functional theory*, Computer Physics Communications, 119 (1999, Jun.) 67-98.

Available:

<https://www.sciencedirect.com/science/article/abs/pii/S001046559800201X>

- [40] W. Kohn, L.J. Sham. *Self-consistent equations including exchange and correlation effects*. Phys. Rev., 140 (1965) A1133.

Available: <http://dx.doi.org/10.1103/PhysRev.140.A1133>

- [41] G. C. Solomon, C. Herrmann, T. Hansen, V. Mujica, M. A. Ratner, *Exploring local currents in molecular junctions*, Nat. Chem., 2 (2010, Mar.) 223-228.

Available: <https://www.nature.com/articles/nchem.546>

- [42] Y. Tsuji, R. Movassagh, S. Datta and R. Hoffmann, *Exponential Attenuation of Through-Bond Transmission in a Polyene: Theory and Potential Realizations*, ACS Nano, 9 (2015, Sep.) 11109-11120.

Available: <https://pubs.acs.org/doi/10.1021/acs.nano.5b04615>